PCCP

PAPER

View Article Online
View Journal | View Issue

Check for updates

Cite this: *Phys. Chem. Chem. Phys.*, 2018, **20**, 15486

Temperature dependence of phonon properties in CVD MoS_2 nanostructures – a statistical approach†

Jarosław Judek, * Arkadiusz P. Gertych, Karolina Czerniak and Mariusz Zdrojek

Received 23rd February 2018,
Accepted 15th May 2018

DOI: 10.1039/c8cp01232f

rsc.li/pccp

In this paper, we report the results of Raman measurements on various molybdenum disulfide (MoS_2) nanostructures grown by the chemical vapor deposition (CVD) method on a typical Si/SiO_2 substrate. The phonon properties investigated include the positions, widths, and intensities of the E_{2g} and A_{1g} modes and the derivative of the mode positions with respect to the temperature in the 300–460 K range. Our results give new insight into changes in phonon energies in response to different disturbances and show that changes induced by the temperature are similar to the changes induced by stress, making these two factors hardly resolvable in the $\hbar\omega_{A_{1g}}$–$\hbar\omega_{E_{2g}}$ coordinate system. We prove that all our samples are weakly coupled to the substrate; thus, the presented results almost purely illustrate the effect of the temperature and thickness. The much stronger coupling to the substrate, however, can explain the high variation in the data reported in the literature. The statistical approach applied makes our results highly reliable and allows proper uncertainty assessment of the obtained results, which is helpful when comparing our results to the results reported by other authors.

Published on 16 May 2018. Downloaded by Politechnika Warszawska on 07/06/2018 11:47:48.

Introduction

Molybdenum disulfide, also called molybdenite in its natural form, is a well-known bulk semiconductor. In the past decade, however, it has been rediscovered as it has surprisingly become clear that materials with a layered crystallographic structure, such as graphene, boron nitride and transition metal dichalcogenides, can exist in a thermodynamically stable state even as one-atom-thick layers.[1] The rapid emergence of a variety of new metallic, semiconducting and dielectric below-1 nm-thick films often possessing unique and desirable properties immediately started discussion of their large-scale production processes. Among the many production methods of MoS_2 monolayers, the most promising and simultaneously the most advanced one is chemical vapor deposition,[2,3] which, however, is still under development. The main disadvantage of CVD is the fact that within a single substrate, many different MoS_2 nanostructures can coexist, including an ideal continuous monolayer, a continuous monolayer with bilayer seeds on the monolayer grain boundaries, isolated monolayer triangles or more complex and thicker isolated nanostructures, all of which are depicted in Fig. 1. Whereas from a technological point of view this situation is highly unacceptable, from a scientific point of view, it is an interesting system, where the influence of the morphology on the structural, thermal, electrical or optical properties can be freely examined.

In this paper, using this inhomogeneous system, we examine one of the properties of thin MoS_2 films – the phonon properties. Phonons are quasi-particles related to the vibrations of atoms constituting crystal lattices. They determine phenomena such as thermal expansion, heat transport, charge carrier mobility, and photoluminescence. To access phonon properties, we use a very powerful, convenient and widely used tool called Raman spectroscopy. In this technique, the result of the measurement is a Raman spectrum, that is, a histogram of energies of photons that have been inelastically scattered by phonons. Analysis of such a spectrum can be used for material identification because phonon energies are a fingerprint of chemical compounds. Much more interesting, however, are the changes in Raman spectra in response to different disturbances, which can have important physical meaning. For example, temperature changes in phonon energies,[4–19] which we investigate in this paper, are primary related to the anharmonicity of the crystal lattice potential. Knowledge of the temperature dependencies of the Raman spectrum also has practical application, for example, in Raman thermometry, where Raman peak positions are correlated with the local temperature, allowing for visualization of the temperature distribution across the sample.[16] Another possibility is the calculation of a material's thermal conductivity (and optionally interfacial thermal conductance) using the

Faculty of Physics, Warsaw University of Technology, Koszykowa 75, 00-662 Warszawa, Poland. E-mail: jaroslaw.judek@pw.edu.pl

† Electronic supplementary information (ESI) available. See DOI: 10.1039/c8cp01232f

This journal is © the Owner Societies 2018

Published on 16 May 2018. Downloaded by Politechnika Warszawska on 07/06/2018 11:47:48.

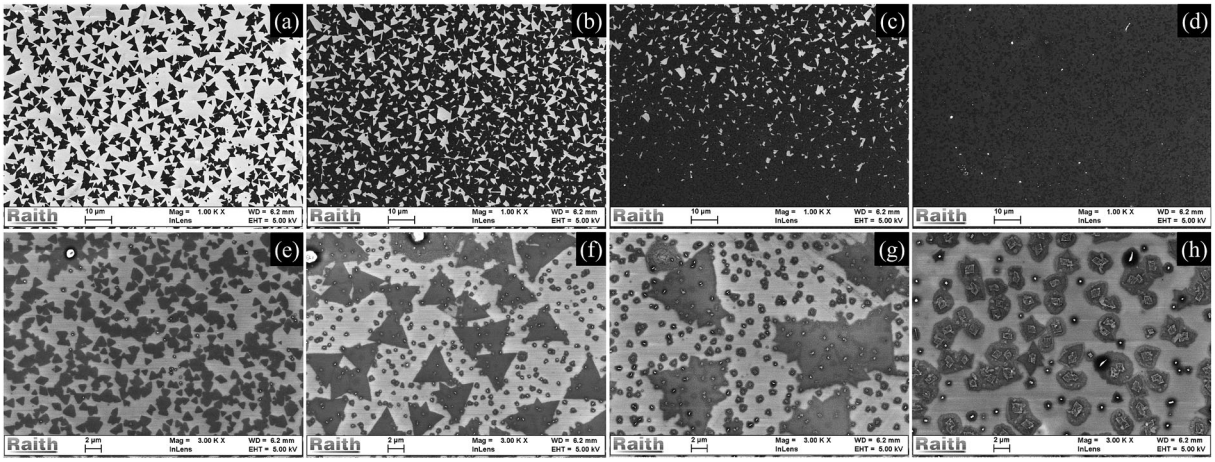

Fig. 1 SEM images of different parts of a sample on which MoS_2 was grown by the CVD technique; (a–d) morphological transformation of the MoS_2 isolated monolayer triangle flakes into a continuous monolayer with bilayer structures at the boundaries; (e–h) transformation of the MoS_2 isolated monolayer triangle flakes into almost isolated multi-layer nanostructures.

Raman optothermal method.[20–26] In this case, the temperature increase indicated by the shifts in the Raman peak positions is correlated with the laser power absorbed by the sample, thus giving information on how effectively the heat generated at the laser spot is evacuated to the rest of the sample.

Shifts in the Raman peak positions can also have causes other than temperature, such as externally applied stress,[27–30] strain related to the substrate,[31,32] doping,[33] and change in the number of layers,[34] all of which can also change within a sample.[35] Therefore, it is important to be able to identify and resolve all contributions to Raman peak position shifts. This task was partially done in the literature but only for stress and doping.[31,32,35] The role of temperature and thickness, which we focus on in this work, is deficient. Our results give new insight into changes in phonon energies in response to different disturbances and show that changes induced by the temperature are similar to the changes induced by stress, making these two causes hardly distinguishable. In particular, using the theoretically calculated MoS_2 thermal expansion coefficient, we demonstrate that the stress induced by the thermal expansion of the substrate could lead to the high variation in results reported in the literature, similar to the case of CVD graphene.[36] We note that the statistical approach applied makes our results highly reliable because we show all data instead of only selected data that match our thesis. Moreover, the adopted methodology allows proper uncertainty assessment of the obtained results, which is helpful when comparing our results to the results reported by other authors.

Samples

The CVD MoS_2 samples were bought from the "2D Semiconductors" company as a 'batch' (several samples from the same process). Some of the samples were found to be not homogenous, and two morphological transformations starting from isolated MoS_2 monolayer triangle flakes were identified. The first type of transformation is shown in Fig. 1a–d. A change in the MoS_2 film morphology from isolated monolayer triangle flakes to a continuous monolayer with bilayer structures at the boundaries is easily noticed. To check whether the nanostructures shown in Fig. 1a are indeed MoS_2 monolayers, we made measurements using atomic force microscopy. The results are presented in Fig. 2a as a topography scan and in Fig. 2b as a height distribution. The average height of the MoS_2 nanostructures was found to be 0.88 nm, which confirms our claim.

The second type of MoS_2 morphological transformation is shown in Fig. 1e–h. Here, the change is related to increasing the number of layers in the individual MoS_2 flakes without forming a continuous layer. Similar multilayer structures have been already observed and identified in the literature, for example, in ref. 37. We present an AFM topography scan in Fig. 2c and the corresponding height distribution in Fig. 2d. As can be seen, the average height of these nanostructures equals ~3 nm, while the maximum height equals approximately 10 nm.

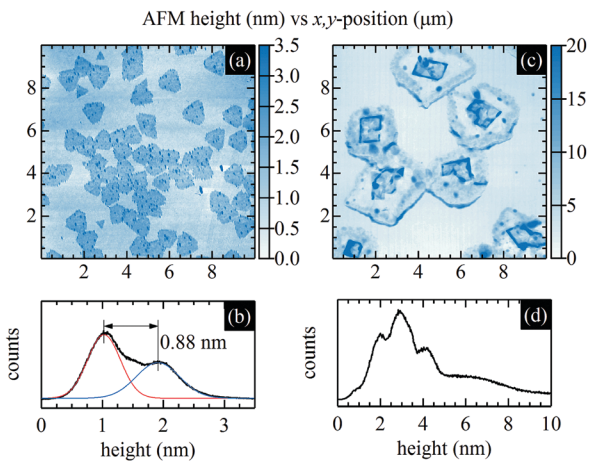

Fig. 2 (a) AFM image of isolated CVD MoS_2 triangle monolayers and the corresponding height distribution (b); the average height of the MoS_2 flakes is 0.88 nm; (c) AFM image of mostly isolated CVD MoS_2 multilayer nanostructures and their height distribution (d); conclusions on the height are not as straightforward as in the case of a monolayer.

Published on 16 May 2018. Downloaded by Politechnika Warszawska on 07/06/2018 11:47:48.

For our study, we selected three areas related to the first morphological transformation (as shown exactly in Fig. 1b–d) and six areas related to the second transformation. This selection arises from the fast changes in phonon properties during the second transformation and the slow changes during the first one.

Experimental

Raman measurements were collected using a Renishaw inVia Raman spectrometer equipped with a motorized XYZ stage for position control (100 nm resolution) and a Linkam DSC600 optical cell system for temperature control (0.1 °C resolution). For excitation, we used a 514 nm laser line (circular polarization, defocused laser beam, laser spot size ~2 μm, laser power ~8 mW). For each temperature and area on the sample (related to different MoS_2 nanostructures), we acquired one Raman map – a set of 169 single measurements ('point spectra') taken on a 13 × 13 square grid, in which neighboring points were located 2 μm from each other. From every 'point spectrum', we extracted the E_{2g} and A_{1g} peak position, width (full width at half maximum), and intensity (area under the peak, not the height), and we calculated the temperature derivatives of the E_{2g} and A_{1g} peak positions – denoted $\chi_{T,E_{2g}}$ and $\chi_{T,A_{1g}}$, respectively. We note that for MoS_2 mono- and multilayers, the Raman spectra include two main peaks called (after the names of irreducible representations) E_{2g} and A_{1g}. Their centers are equal to the phonon energies taken at the center of the Brillouin zone (the Γ point), and the widths of the peaks are related to both phonon lifetimes and sample inhomogeneity within the illuminating laser spot. All measurements were taken in air for five substrate temperatures (T = 300 K, 340 K, 380 K, 420 K, and 460 K) from the highest temperature to the lowest one. Before measurement, samples were annealed at 460 K for one hour in order to exclude any transient issues.

Results

The results of Raman measurements on MoS_2 nanostructures during the first type of morphological transformation are presented in Fig. 3. The E_{2g} and A_{1g} phonon energies are shown in Fig. 3a in the $\hbar\omega_{A_{1g}}$–$\hbar\omega_{E_{2g}}$ coordinate system for five substrate temperature values for three different areas on the sample. Data are depicted as points with error bars. The point coordinates are taken as the average of the phonon energies for a specified temperature and area on the sample, and the lengths of the error bars are the standard deviations of the corresponding phonon energy distributions. We note that the $\hbar\omega_{A_{1g}}$–$\hbar\omega_{E_{2g}}$ coordinate system used here is analogous to the one often used in the case of graphene, the $\hbar\omega_{2D}$–$\hbar\omega_{G}$ coordinate system, which is convenient when analyzing contributions to the Raman spectra from doping, stress and temperature.[36,38]

Regarding the interpretation of the results, the first detail to see in Fig. 3a is that the E_{2g} and A_{1g} phonon energies are correlated within each data series. The linear dependence between phonon energies is quite intuitive since the dependence of the Raman mode position on temperature is often approximated by the linear relation $\hbar\omega(T) = \chi_T \cdot T + \omega_0$, and hence, $\Delta\hbar\omega_{A_{1g}}/\Delta\hbar\omega_{E_{2g}} = \chi_{T,A_{1g}}/\chi_{T,E_{2g}}$.

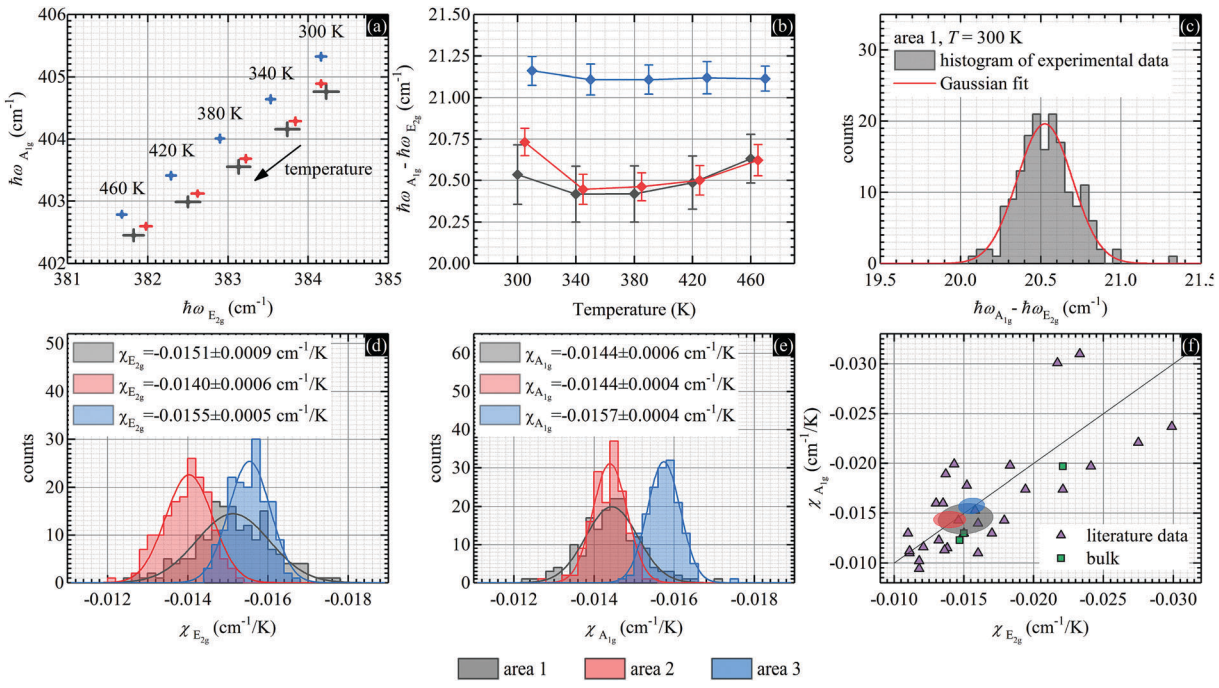

Fig. 3 (a) Temperature dependence of the E_{2g} and A_{1g} phonon energies for three specified positions on the sample; (b) difference between A_{1g} and E_{2g} phonon energies as a function of temperature; (c) an exemplary histogram of the phonon energy differences for a selected position and temperature; (d and e) histograms of the temperature derivatives of the E_{2g}/A_{1g} phonon energies for three previously specified positions on the sample; (f) our results collated with the data reported in the literature.

 This journal is © the Owner Societies 2018

Published on 16 May 2018. Downloaded by Politechnika Warszawska on 07/06/2018 11:47:48.

The ratio of changes in the A_{1g} mode position to changes in the E_{2g} mode position for all series in Fig. 3a is close to ~ 1. This is an important result because compressive biaxial strain was reported to cause shifts in the Raman E_{2g} and A_{1g} peak positions with a ratio close to ~ 0.67,[29] whereas hole doping was reported to give shifts with a ratio close to 6.7.[33] Therefore, temperature and stress contributions to Raman shifts are similar to each other and thus could hardly be resolved in the $\hbar\omega_{A_{1g}}$–$\hbar\omega_{E_{2g}}$ coordinate system. Moreover, temperature-induced changes in the Raman spectra from the supported MoS_2 samples depend not only on the properties of MoS_2 but also on the thermal expansion of the substrate.[36] This issue, however, will be discussed separately further.

Next, we address the spread of the experimental data. As can be noticed, the first series in Fig. 3a is the most widely distributed. This is because within the defocused laser spot, the coverage of the surface by the MoS_2 nanostructures is the smallest, which results in the lowest signal intensity and thus the lowest precision of the data extraction procedure. We note that the uncertainty of the peak position value depends not only on the spectrometer resolution but also on the intensity of the Raman signal, which is subjected to the numerical fitting procedure. Thus, the lower the Raman signal-to-noise ratio, the higher the variation in the extracted phonon parameters. The distribution of the data in the second and third series is much narrower, which we attribute simply to the much higher Raman signal-to-noise ratio.

The data in the second series are close to the data in the first one, but the data in the third series are substantially shifted with respect to the previous series in a direction 'orthogonal' to the changes induced by the temperature. We attribute this interesting shift to the emergence of the bilayer structure at grain boundaries in the MoS_2 monolayer. To validate this statement, we examined the difference between the A_{1g} and E_{2g} phonon energies, which is considered to be a convenient and reliable indicator of the number of MoS_2 layers.[34] The A_{1g} and E_{2g} phonon energy differences as a function of temperature for each of the areas are plotted in Fig. 3b. The data follow expectations – the phonon energy differences for the third area are larger than those for the first and second area, which are close to each other. The temperature influence on the phonon energy difference is minor when taking the uncertainties into account, but for the first and second area on the sample, the value for the lowest temperature seems to be a little higher. We note that the value of the phonon energy differences is calculated as the average of each difference, whereas the errors bars represent the standard deviation of the differences. A histogram of calculated differences between the A_{1g} and E_{2g} phonon energies for a selected area (the first one – the most sparse monolayer triangles) and a selected temperature of the substrate (T = 300 K) is shown in Fig. 3c. The Gaussian function well approximates the experimental data, proving the normal distribution of the results. This means that there is no proof that there exists a specific cause of the phonon energy divergence and that the data variation results from the measurement uncertainty and sample inhomogeneity.

Fig. 3d and e illustrate the evolution of the distributions of the temperature derivatives of the E_{2g} and A_{1g} phonon energies during the first morphological transformation of the MoS_2 film. As mentioned previously, the data for the first area are the most widely distributed. What is interesting is the non-negligible difference between χ_T values, for both the E_{2g} and A_{1g} modes, for the second and third areas. This difference is related to the transformation of the MoS_2 layer from an almost continuous and full monolayer to a fully continuous monolayer with some bilayers at the boundaries. To obtain a wider perspective, we collate our results and literature data in the $\chi_{T,A_{1g}}$–$\chi_{T,E_{2g}}$ coordinate system (convenient when searching for some correlations) in Fig. 3f. The exact literature values taken for this figure are listed in Table 1. The ellipses represent the distributions of our results, assuming that the semi-minor and semi-major axis lengths are equal to two times the standard deviation of our data. As one can see, the first set of data (the gray one) is the largest one due to the highest measurement uncertainties. The second and third sets of data (the red and blue ones) are more confined, and even more importantly, they are separated. Thus, the structural change in the MoS_2 layer was reflected in the χ_T value distributions. We also note that the variation in our lowest-confidence data (acquired in the first position) is still much lower than the variation in all the data reported to date in the literature, which is somewhat incomprehensible. A possible explanation for the change in χ_T value and the high variability of the literature data will be discussed further.

Fig. 4 shows analysis of the phonon properties conducted for the second morphological transformation – from isolated monolayer triangle flakes to isolated multilayer flakes. Fig. 4a illustrates distributions in the E_{2g} and A_{1g} phonon energies for five substrate temperature values for six areas. It is striking that the data are twofold correlated.

First, similar to the case of the first morphological transformation, the E_{2g} and A_{1g} phonon energies for each area demonstrate linear dependence with slope ~ 1. The average value obtained using the Deming orthogonal regression method equals: $\Delta\hbar\omega_{A_{1g}}/\Delta\hbar\omega_{E_{2g}} = 0.99 \pm 0.13$ and does not depend on the area within uncertainty limits. This means that the temperature derivatives of the E_{2g} and A_{1g} mode positions $\chi_{T,E_{2g}}$ and $\chi_{T,A_{1g}}$ are approximately equal regardless of the thickness of the flakes.

Second, the linear dependence between the E_{2g} and A_{1g} phonon energies can be identified for a constant temperature and for different areas (thicknesses, number of layers). In Fig. 4a, this change is illustrated as a shift in the data in a direction 'orthogonal' to the changes induced by the temperature. The average slope of the line that best fits the experimental data and is obtained using a weighted total least-squares algorithm[39] equals: $\Delta\hbar\omega_{A_{1g}}/\Delta\hbar\omega_{E_{2g}} = -2.81 \pm 0.32$. We note that this slope does not depend on the temperature in the 300–460 K temperature range; thus, it is a reliable indicator allowing separation of thickness from doping and stress/temperature.

In Fig. 4b, we plot the A_{1g} and E_{2g} phonon energy differences as a function of temperature for each of the areas. The data follow expectations – the phonon energy differences increase in value as the nanostructures became thicker. Moreover, the

Published on 16 May 2018. Downloaded by Politechnika Warszawska on 07/06/2018 11:47:48.

Table 1 Values of the temperature derivative of the E_{2g} and A_{1g} phonon energies reported in the literature

Material	$\chi_{E_{2g}}$ value (cm^{-1} K^{-1})	$\chi_{A_{1g}}$ value (cm^{-1} K^{-1})	Temperature range	Ref.
Bulk	−0.0147(5)	−0.0123(5)	95–573 K	4
Bulk	−0.015	−0.013	293–453 K	5
Mono, CVD, Si/SiO_2	−0.013	−0.016		
Few-layer, vapor-phase, Si/SiO_2	−0.0132	−0.0123	83–523 K	6
Mono, mechanical exfoliation, Si/SiO_2	−0.0179(9)	−0.0143(7)	300–550 K	7
Bi, mechanical exfoliation, Si/SiO_2	−0.0137(9)	−0.0189(3)		
Mono, CVD, Si/SiO_2	−0.0138	−0.0115		
Mono, mechanical exfoliation, suspended	−0.011(1)	−0.013(1)	100–320 K	8
Mono, mechanical exfoliation, sapphire	−0.017	−0.013		
Mono, mechanical exfoliation, Si/SiO_2	−0.0152	−0.0178	70–350 K	9
Few-layer, hydrothermal, freestanding	−0.016	−0.011	77–623 K	10
Bulk	−0.0221 ± 0.0009	−0.0197 ± 0.0009	25–500 °C	11
Mono, mechanical exfoliation, Si/SiO_2	−0.0241 ± 0.0015	−0.0626 ± 0.0038		
Mono, CVD, Si/SiO_2	−0.0217 ± 0.0017	−0.0301 ± 0.0023	25–400 °C	
Bi, CVD, Si/SiO_2	−0.0233 ± 0.0018	−0.0310 ± 0.0018		
Mono, CVD, sapphire	−0.0143 ± 0.0006	−0.0199 ± 0.0012	25–425 °C	
Bi, CVD, sapphire	−0.0135 ± 0.0008	−0.0160 ± 0.0014		
Mono, mechanical exfoliation, supported	—	−0.0167 ± 0.0007	300–500 K	12
Bi, mechanical exfoliation, supported	—	−0.0139 ± 0.0005		
Mono, mechanical exfoliation, suspended	—	−0.0203 ± 0.0006		
Bi, mechanical exfoliation, suspended	—	−0.0141 ± 0.0004		
Mono, CVD, Si/SiO_2	−0.0136	−0.0113	80–593 K	13
Mono, CVD, Si/SiO_2	−0.0121	−0.0116	90–540 K	14
Bi, CVD, Si/SiO_2	−0.0118	−0.00941		
Multi, CVD, Si/SiO_2	−0.0118	−0.0102		
7-Layer, mechanical exfoliation, Si	−0.0146 ± 0.0004	−0.0143 ± 0.0005	292–415 K	15
8-Layer, mechanical exfoliation, Si	−0.0111 ± 0.0004	−0.0110 ± 0.0005		
13-Layer, mechanical exfoliation, Si	−0.0158 ± 0.0008	−0.0153 ± 0.0014		
20-Layer, mechanical exfoliation, Si	−0.0299 ± 0.0019	−0.0237 ± 0.0013		
33-Layer, mechanical exfoliation, Si	−0.221	−0.0174 ± 0.0013		
47-Layer, mechanical exfoliation, Si	−0.275 ± 0.0015	−0.0221 ± 0.0013		
75-Layer, mechanical exfoliation, Si	−0.0194 ± 0.0012	−0.0174 ± 0.0010		
Mono, CVD, Si/SiO_2	−0.015 ± 0.002	−0.013 ± 0.001	RT–250 °C	16
Mono, CVD, Si/SiO_2	−0.0183 ± 0.0009	−0.0198 ± 0.0014	RT–305 °C	17
Mono, CVD, Si/SiO_2 + WS_2 on top	−0.0111 ± 0.0003	−0.0112 ± 0.0002	300–642 °C	18
Mono, mechanical exfoliation, Si/SiO_2	−0.016	−0.014	175–575 K	19
Mono, noncontiguous, CVD, Si/SiO_2	−0.0140 ± 0.0006	−0.0144 ± 0.0004	300–460 K	This work
Mono + bi, CVD, Si/SiO_2	−0.0155 ± 0.0005	−0.0157 ± 0.0004		
Various isolated MoS_2 few layers, CVD, Si/SiO_2	−0.0144 ± 0.0007	−0.0144 ± 0.0007		

phonon energy differences do not change significantly with temperature. This suggests that phonon energy difference is a good indicator of the number of layers for all temperatures in the 300–460 K temperature range. A histogram of calculated differences between the A_{1g} and E_{2g} phonon energies for a selected area (the first one) and a selected temperature of the substrate (T = 300 K) is shown in Fig. 4c. The Gaussian function well approximates the experimental data, proving the normal distribution of the results. The average values of the phonon energy differences with corresponding standard deviations calculated for each area on the sample are illustrated in Fig. 4d. The values of the standard deviation in this case are related to the dynamics of the transformation within the scanned area – the faster changes, the greater the variation in the data.

In Fig. 4e, we present the average value of the temperature derivatives of the E_{2g} and A_{1g} phonon energies for each area, supplemented with the standard deviation values depicted as error bars. We note that despite the adopted statistical approach, no clear trend in the provided data can be identified. In particular, the variation in the acquired data is so high that it

 This journal is © the Owner Societies 2018

Published on 16 May 2018. Downloaded by Politechnika Warszawska on 07/06/2018 11:47:48.

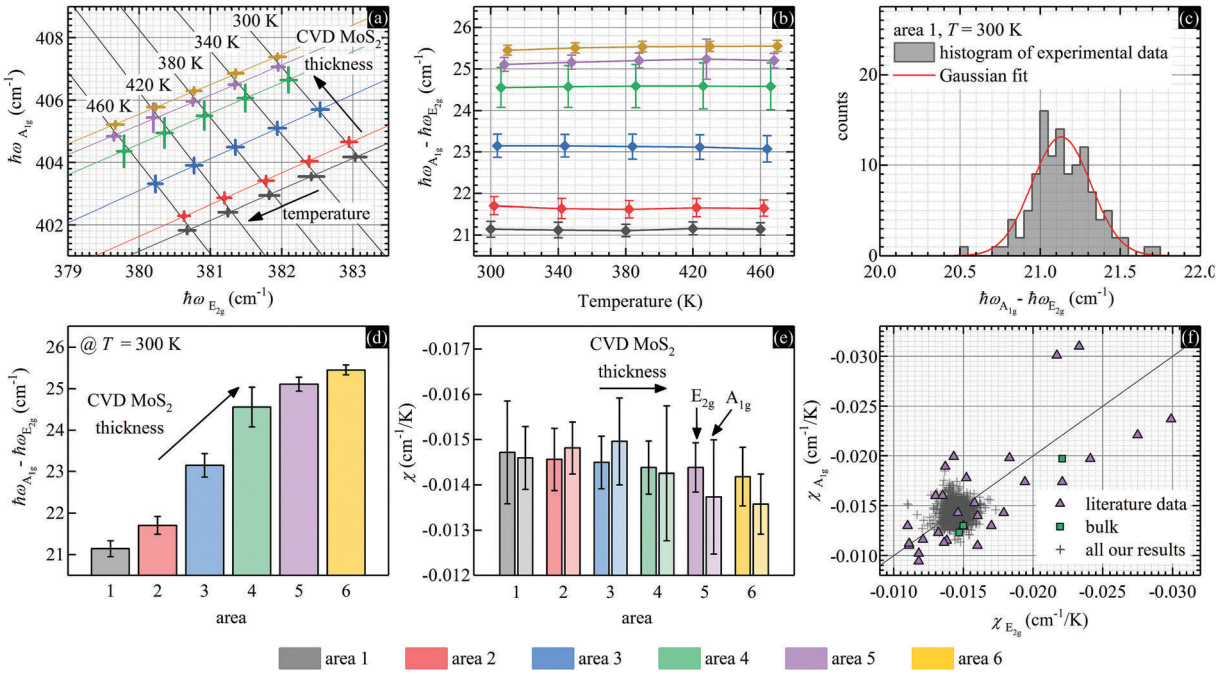

Fig. 4 (a) Temperature dependence of the E_{2g} and A_{1g} phonon energies for six specified positions on the sample; (b) difference between the A_{1g} and E_{2g} phonon energies as a function of temperature; (c) an exemplary histogram of the phonon energy differences for a selected position and temperature; (d) dependence of the average phonon energy difference on the place on the sample, where the error bars denote the standard deviation; (e) temperature derivative of the phonon energy for six places on the sample, where the error bars denote the standard deviation; (f) our results collated with the data reported in the literature.

completely outmatches minor changes that were expected to have been identified during the clearly seen structural transformation. Therefore, there is no proof that a correlation exists between the temperature derivative of the E_{2g} and A_{1g} mode positions and the thickness of the sample. Finally, in Fig. 4f, we collate the literature data with our data acquired during the second transformation, which for clarity were pooled together into one data set. We note that variation in our data, as mentioned previously, is much lower than the variation in all the data reported to date in the literature. This issue will be discussed further.

To demonstrate that the linear dependence between the E_{2g} and A_{1g} mode positions with slope ~ 1 can also be found in the results of other Raman measurements in which the temperature of the sample is changing, we analyzed our data obtained for multilayer exfoliated MoS_2 flakes.[26] First, we check the data for different substrate temperatures and laser powers. We note that the local temperature of samples investigated using Raman spectroscopy depends not only on the temperature of the substrate but also on the heating by the incident laser beam. When the laser power density is small, the laser heating of the sample can often be neglected. As a consequence, the temperature distribution within the laser spot is homogenous and is equal to the temperature of the substrate. However, for higher laser powers, a significant temperature increase in the probed sample could occur. In this case, the temperature increase is nonhomogeneous and depends on the thermal conductivity κ of the sample, on the interfacial thermal conductance g between the sample and the substrate, and on the distribution of the laser power density. Moreover, laser heating of the sample is usually limited to a small part of the whole system; in particular, it does not change the temperature of the substrate. Fig. 5a and b show the results. The E_{2g} and A_{1g} mode positions for four different laser powers for five different substrate temperatures are shown in Fig. 5a. The same data in the $\hbar\omega_{A_{1g}}$–$\hbar\omega_{E_{2g}}$ coordinate system are shown in Fig. 5b. All experimental points are clearly placed on a straight line with a slope that equals 0.93, which is in agreement with our previous results.

The second analysis concerns changes in laser power density distribution. In this case, the temperature of the substrate and the laser power are constant, but the beam size is changing. We realized this by changing the distance between the sample surface and the laser beam waist. Further details can be found in ref. 26. In Fig. 5c, we show derivatives of the E_{2g} and A_{1g} mode positions with respect to the laser power *versus* distance of the sample surface from the laser beam waist for a substrate temperature that equals 300 K. We note that the temperature distribution within the laser spot is also nonhomogeneous and depends on κ and g and that the temperature of the substrate usually does not increase. Fig. 5d illustrates data in the $\partial\hbar\omega_{A_{1g}}/\partial P_L$–$\partial\hbar\omega_{E_{2g}}/\partial P_L$ coordinate system, and similar to Fig. 5b, all experimental points are placed on a straight line with a slope that equals 1.17, which further confirms our findings. We note that all lines in the $\hbar\omega_{A_{1g}}$–$\hbar\omega_{E_{2g}}$ and $\partial\hbar\omega_{A_{1g}}/\partial P_L$–$\partial\hbar\omega_{E_{2g}}/\partial P_L$ coordinate systems are fitted using the Deming orthogonal method instead of using the standard regression method because both $\hbar\omega_{A_{1g}}$ and $\hbar\omega_{E_{2g}}$ have comparable uncertainties and neither of them can be neglected. The small deviation in the slope of the

Published on 16 May 2018. Downloaded by Politechnika Warszawska on 07/06/2018 11:47:48.

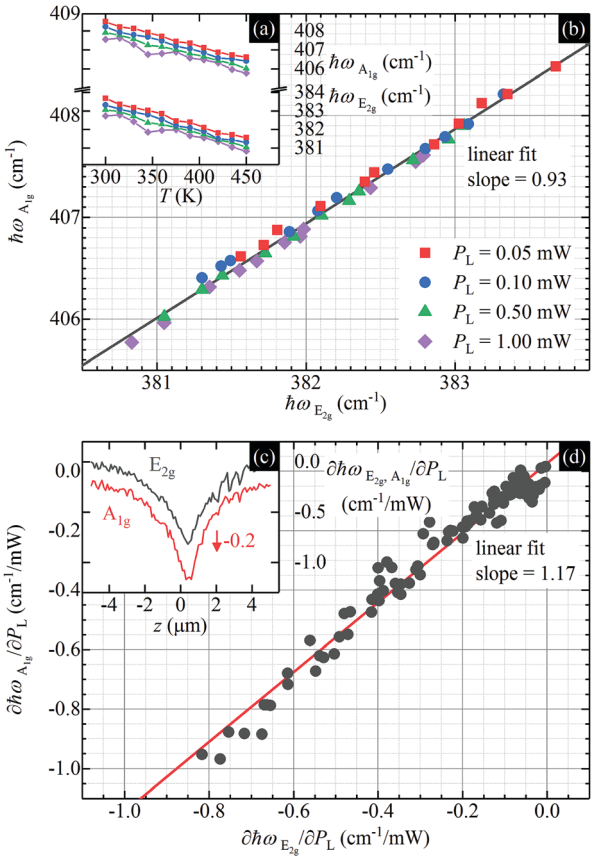

Fig. 5 Raman peak position as a function of temperature of the substrate for four laser power values (a) and in the $\hbar\omega_{A_{1g}}$–$\hbar\omega_{E_{2g}}$ coordinate system (b); Raman peak positions as a function of the distance between the sample surface and the focus of the laser beam (c) and in the $\partial\hbar\omega_{A_{1g}}/\partial P_L$–$\partial\hbar\omega_{E_{2g}}/\partial P_L$ coordinate system (d). All data from ref. 26.

fitted line from a value ~1 results from 'point measurements' in our previous work.[26]

The last question we discuss in this paper is the influence of substrate thermal expansion on the temperature derivatives of the mode positions χ_T and their correlations.[36] At the beginning, we note that the linear thermal expansion coefficient calculated for a MoS_2 monolayer $\alpha_{MoS_2} = 17.4 \times 10^{-6}$ K^{-1},[19,40] whereas the linear thermal expansion coefficient for a bulk silicon substrate $\alpha_{Si} \sim 2.56 \times 10^{-6}$ K^{-1}.[41] The large mismatch between thermal expansion coefficients (TECs) could lead to temperature-dependent stress in the sample. This situation is possible when a sample is strongly coupled to the substrate and mimics its thermal expansion. The value of the temperature-dependent contribution to stress can be written as:

$$\varepsilon_{TEC}(\Delta T) = c\cdot(\alpha_{Si} - \alpha_{MoS_2})\cdot\Delta T, \quad c \in \langle 0;1\rangle, \qquad (1)$$

where ΔT stands for the temperature difference and c describes the coupling of the MoS_2 nanostructure to the substrate; namely, it says whether a MoS_2 nanostructure follows its own thermal expansion or mimics the thermal expansion of the substrate. This substrate-induced strain ε will be biaxial and compressive since $\alpha_{MoS_2} > \alpha_{Si}$. In the case when the MoS_2 nanostructures are initially tensile strained, the substrate-induced stress induced by the temperature increase will decrease its value. Such a situation could take place for samples grown using the CVD technique, for which the bonding between the MoS_2 and the substrate is formed at the growth temperature, much higher than room temperature. Assuming that MoS_2 film is relaxed at the growth temperature, the subsequent cooling will produce significant tensile strain at room temperature resulting in TEC mismatch, which was discussed by Su *et al.*[11,17,42]

Now, assuming that the data obtained during the first morphological transformation in the second area represent a MoS_2 flake that is weakly coupled to the substrate (c = 0), the sample can follow unconstrained thermal expansion despite completely different thermal expansion coefficients of the substrate. Formally:[43]

$$\chi_T = \left(\frac{\partial\hbar\omega}{\partial T}\right)_V + \left(\frac{\partial V}{\partial T}\right)_p \cdot \left(\frac{\partial\hbar\omega}{\partial V}\right)_T \qquad (2)$$

Next, let's calculate the $\chi_{T,E_{2g}}'$ and $\chi_{T,A_{1g}}'$ values assuming that the flake is fully coupled to the substrate (c = 1) and that χ_T does not depend much on the externally applied strain. Formally:

$$\chi_T' = \chi_T + c\cdot\frac{\partial\hbar\omega}{\partial\varepsilon}\cdot\frac{\partial\varepsilon}{\partial T} = \chi_T + \frac{\partial\hbar\omega}{\partial\varepsilon}\cdot 1\cdot(\alpha_{Si} - \alpha_{MoS_2}). \qquad (3)$$

Taking $\Delta\hbar\omega_{E_{2g}} = \sim 3$ cm^{-1} and $\Delta\hbar\omega_{A_{1g}} = \sim 2$ cm^{-1} for $\Delta\varepsilon = -0.2\%$,[29] we obtained $\chi_{T,E_{2g}}' = \chi_{T,E_{2g}} + 0.0223$ cm^{-1} K^{-1} and $\chi_{T,A_{1g}}' = \chi_{T,A_{1g}} + 0.0148$ cm^{-1} K^{-1}. It can be seen that the change in the $\chi_{T,E_{2g}}$ and $\chi_{T,A_{1g}}$ values obtained for no coupling and for full coupling of the MoS_2 flake to the substrate is of the same order as the scale of the variation in all the literature data. Thus, different coupling of the MoS_2 flake to the substrate, which means different strain resulting from TEC mismatch, can partially explain the large variation in the literature data. The straight yellow line illustrates different contributions from the thermal expansion of the substrate to the temperature derivatives of the phonon energies. Its slope equals the ratio of the derivative of the A_{1g} phonon energy with respect to strain to the derivative of the E_{2g} phonon energy with respect to strain, which is: $(\Delta\hbar\omega_{A_{1g}}/\Delta\varepsilon)/(\Delta\hbar\omega_{E_{2g}}/\Delta\varepsilon) \sim 0.67$. To include dispersion in the $\partial\hbar\omega/\partial\varepsilon$ values, we assumed that the above slope can vary by 25%, which is marked in Fig. 6 as a yellow streak. Within this area, not only all our data, denoted as 'rest of results', but also most of the literature data are placed. We note that initial strain inside the MoS_2 nanostructures does not contribute to the temperature derivatives of the mode energies because the temperature derivative includes only those contributions which are temperature-dependent. Thus, it is not important at what temperature the MoS_2 nanostructures were relaxed, what is only important is the coupling to the substrate. If the strength of the coupling is changing in subsequent heating–cooling cycles, the $\chi_{T,E_{2g}}$ and $\chi_{T,A_{1g}}$ values will obviously change. We emphasize that we report results that do not change during the heating–cooling cycles, therefore the samples considered here are somehow relaxed.

Contribution of the substrate-induced strain in the proposed explanation will always lead to a decrease in the $\chi_{T,E_{2g}}$ and $\chi_{T,A_{1g}}$ absolute values since both are negative. Therefore, the fact that

 This journal is © the Owner Societies 2018

Published on 16 May 2018. Downloaded by Politechnika Warszawska on 07/06/2018 11:47:48.

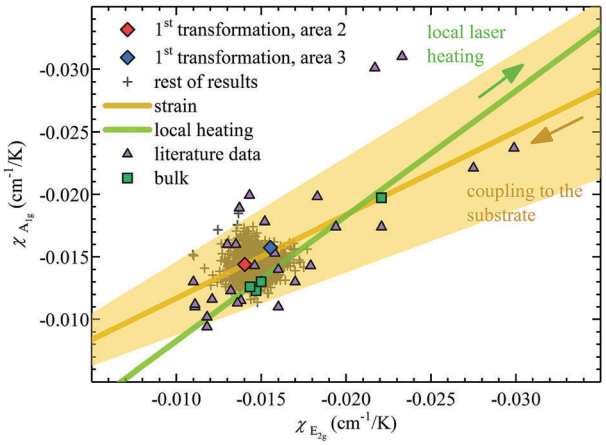

Fig. 6 Derivative of the A_{1g} mode position with respect to temperature *vs.* derivative of the E_{2g} mode position with respect to temperature. The yellow line represents the contribution from strain resulting from thermal expansion of the substrate. Its glow represents the 25% uncertainty margin. The green line represents the contribution from local laser heating of the sample that depends on the thermal conductivity κ and the thermal interface conductance g.

some of the reported values are larger in magnitude requires some comment. We identified two causes that can lead to the increase in the magnitude of the $\chi_{T,E_{2g}}$ and $\chi_{T,A_{1g}}$. The first one is related to the film–substrate bonding which could be non-stationary under thermal stress.[17] Typically, it is reported as the difference in χ values for subsequent heating–cooling cycles. For example, Su *et al.* in ref. 17 reported that the $\chi_{T,E_{2g}}$ value is changing from -0.0192 cm^{-1} K^{-1} in the first cycle to -0.0183 cm^{-1} K^{-1} in the second cycle, and the $\chi_{T,A_{1g}}$ value is changing from -0.0390 cm^{-1} K^{-1} in the first cycle to -0.0198 cm^{-1} K^{-1} in the second cycle. The change in the $\chi_{T,A_{1g}}$ value is impressive. The second cause is more subtle and is related to the experimental details. Raman spectroscopy uses illumination by the laser beam. Absorption of some part of the incident radiation always leads to an increase in local temperature. This temperature increase is nonhomogeneous within the laser spot and depends on the heat dissipation effectiveness, which at least partially depends on the thermal conductivity κ and the interface thermal conductance g. If this temperature increase is of the same order as the changes in substrate temperature during the study and the heat dissipation depends on the substrate temperature (for example κ depends on the temperature) the χ values will be affected. For example, if the local temperature increase depends mainly on the thermal conductivity, which decreases with temperature, the χ values will be overestimated. This effect is illustrated in Fig. 6 as the green line. Its slope was calculated from the data shown in Fig. 5a. We note that none of the effects described above take place in our work.

From this perspective, it is valuable to discuss again the results presented in Fig. 3–5. During the first morphological transformation, the MoS_2 film starts to be continuous. As a result, a non-negligible change in $\chi_{T,E_{2g}}$ and in $\chi_{T,E_{2g}}$ is observed. A possible explanation is that the continuous part of the MoS_2 film is less coupled to the substrate and thus is exposed to a slightly lower compressive strain contribution than the non-contiguous part. The difference in the coupling constant $\Delta c = 0.077$. During the second morphological transformation, the MoS_2 isolated flakes became thicker. Assuming that the coupling to the substrate is low (the average values of $\chi_{T,E_{2g}}$ and $\chi_{T,E_{2g}}$ are close to the bulk counterparts), the number of layers does not change the strain acting on the sample as a whole,[44,45] because there is no strain transfer from the substrate to the sample. The results presented in Fig. 5 are obtained from mechanically exfoliated multilayer MoS_2 flakes. Because the interfacial thermal conductance is low (lower than values reported in the literature[16]), one can conclude that the coupling to the substrate is also low and that the expansion of the substrate does not affect the expansion of the sample. Thus, the laser heating of the sample has the same effect as external heating of the substrate because both neglect strain resulting from the TEC mismatch. In summary, all our samples are weakly coupled to the substrate, and the presented results illustrate almost purely the effect of the temperature and thickness. The much stronger coupling to the substrate, however, can explain the high variation in the data reported in the literature.

Conclusions

In this paper, we analyzed the correlation between MoS_2 Raman peak positions as a function of the temperature and thickness. We showed that strain and temperature are similar to each other and that it is hard to resolve both contributions to the Raman spectra even in the $\hbar\omega_{A_{1g}}$–$\hbar\omega_{E_{2g}}$ coordinate system. We showed that thermal expansion of the substrate could lead to temperature-dependent strain and thus could significantly affect the temperature derivatives of the phonon energies. It could also partially explain differences in data reported in the literature, even though our results are not affected. We also note the importance of the statistical approach, which includes sample inhomogeneity as well and is absolutely required to provide reliable data, to perform a proper uncertainty assessment and to assign proper meaning to the differences in values reported in the literature.

Conflicts of interest

There are no conflicts to declare.

Acknowledgements

This work was funded by the National Science Centre, Poland, within Project No. 2014/15/D/ST5/03944 and by The National Center for Research and Development, Poland, within Project No. Lider/180/L-6/14/NCBR/2015.

Notes and references

1 K. S. Novoselov, D. Jiang, F. Schedin, T. J. Booth, V. V. Khotkevich, S. V. Morozov and A. K. Geim, Two-dimensional

Published on 16 May 2018. Downloaded by Politechnika Warszawska on 07/06/2018 11:47:48.

atomic crystals, *Proc. Natl. Acad. Sci. U. S. A.*, 2005, **102**, 10451.
2 Y. Zhan, Z. Liu, S. Najmaei, P. M. Ajayan and J. Lou, Large-area vapor-phase growth and characterization of MoS_2 atomic layers on a SiO_2 substrate, *Small*, 2012, **8**, 966.
3 Y.-H. Lee, X.-Q. Zhang, W. Zhang, M.-T. Chang, C.-T. Lin, K.-D. Chang, Y.-C. Yu, J. T.-W. Wang, C.-S. Chang, L.-J. Li and T.-W. Lin, Synthesis of large-area MoS_2 atomic layers with chemical vapor deposition, *Adv. Mater.*, 2012, **24**, 2320.
4 T. Livenh and E. Sterer, Resonant Raman scattering at exciton states tuned by pressure and temperature in 2H-MoS_2, *Phys. Rev. B: Condens. Matter Mater. Phys.*, 2010, **81**, 195209.
5 N. A. Lanzillo, A. G. Birdwell, M. Amani, F. J. Crowne, P. B. Shah, S. Najmaei, Z. Liu, P. M. Ajayan, J. Lou, M. Dubey, S. K. Nayak and T. P. O'Regan, Temperature-dependent phonon shifts in monolayer MoS_2, *Appl. Phys. Lett.*, 2013, **103**, 093102.
6 S. Sahoo, A. P. S. Gaur, M. Ahmadi, M. J.-F. Guinel and R. S. Katiyar, Temperature-Dependent Raman Studies and Thermal Conductivity of Few-Layer MoS_2, *J. Phys. Chem. C*, 2013, **117**, 9042.
7 S. Najmaei, P. M. Ajayan and J. Lou, Quantitative analysis of the temperature dependency in Raman active vibrational modes of molybdenum disulfide atomic layers, *Nanoscale*, 2013, **5**, 9758.
8 R. Yan, J. R. Simpson, S. Bertolazzi, J. Brivio, M. Watson, X. Wu, A. Kis, T. Luo, A. R. Hight Walker and H. G. Xing, Thermal conductivity of monolayer molybdenum disulfide obtained from temperature-dependent Raman spectroscopy, *ACS Nano*, 2014, **8**, 986.
9 A. Taube, J. Judek, C. Jastrzębski, A. Dużyńska, K. Świtkowski and M. Zdrojek, Temperature-dependent nonlinear phonon shifts in a supported MoS_2 monolayer, *ACS Appl. Mater. Interfaces*, 2014, **6**, 8959.
10 M. Thripuranthaka, R. V. Kashid, C. S. Rout and D. J. Late, Temperature dependent Raman spectroscopy of chemically derived few layer MoS_2 and WS_2 nanosheets, *Appl. Phys. Lett.*, 2014, **104**, 081911.
11 L. Su, Y. Zhang, Y. Yu and L. Cao, Dependence of coupling of quasi 2-D MoS_2 with substrates on substrate types, probed by temperature dependent Raman scattering, *Nanoscale*, 2014, **6**, 4920.
12 X. Zhang, D. Sun, Y. Li, G.-H. Lee, X. Cui, D. Chenet, Y. You, T. F. Heinz and J. C. Hone, Measurement of Lateral and Interfacial Thermal Conductivity of Single- and Bilayer MoS_2 and $MoSe_2$ Using Refined Optothermal Raman Technique, *ACS Appl. Mater. Interfaces*, 2015, **7**, 25923.
13 A. S. Pawbake, M. S. Pawar, S. R. Jadkar and D. J. Late, Large area chemical vapor deposition of monolayer transition metal dichalcogenides and their temperature dependent Raman spectroscopy studies, *Nanoscale*, 2016, **8**, 3008.
14 T. Yang, X. Huang, H. Zhou, G. Wu and T. Lai, Excitation mechanism of A_{1g} mode and origin of nonlinear temperature dependence of Raman shift of CVD-grown mono- and few-layer MoS_2 films, *Opt. Express*, 2016, **24**, 12281.
15 P. Yuan, C. Li, S. Xu, J. Liu and X. Wang, Interfacial thermal conductance between few to tens of layered-MoS_2 and c-Si: Effect of MoS_2 thickness, *Acta Mater.*, 2017, **122**, 152.
16 E. Yalon, C. J. McClellan, K. K. H. Smithe, M. M. Rojo, R. L. Xu, S. V. Suryavanshi, A. J. Gabourie, C. M. Neumann, F. Xiong, A. B. Farimani and E. Pop, Energy Dissipation in Monolayer MoS_2 Electronics, *Nano Lett.*, 2017, **17**, 3429.
17 L. Su, Y. Yu, L. Cao and Y. Zhang, *In Situ* Monitoring of the Thermal-Annealing Effect in a Monolayer of MoS_2, *Phys. Rev. Appl.*, 2017, **7**, 034009.
18 Z. Hu, Y. Bao, Z. Li, Y. Gong, R. Feng, Y. Xiao, X. Wu, Z. Zhang, X. Zhu, P. M. Ajayan and Z. Fang, Temperature dependent Raman and photoluminescence of vertical WS_2/MoS_2 monolayer heterostructure, *Sci. Bull.*, 2017, **62**, 16.
19 M. Yang, X. Cheng, Y. Li, Y. Ren, M. Liu and Z. Qi, Anharmonicity of monolayer MoS_2, $MoSe_2$, and WSe_2: A Raman study under high pressure and elevated temperature, *Appl. Phys. Lett.*, 2017, **110**, 093108.
20 I. Calizo, A. A. Balandin, W. Bao, F. Miao and C. N. Lau, Temperature Dependence of the Raman Spectra of Graphene and Graphene Multilayers, *Nano Lett.*, 2007, **7**, 2645.
21 A. A. Balandin, S. Ghosh, W. Bao, I. Calizo, D. Teweldebrhan, F. Miao and C. N. Lau, Superior Thermal Conductivity of Single-Layer Graphene, *Nano Lett.*, 2008, **8**, 902.
22 W. Cai, A. L. Moore, Y. Zhu, X. Li, S. Chen and L. Shi, *et al.*, Thermal transport in suspended and supported monolayer graphene grown by chemical vapor deposition, *Nano Lett.*, 2010, **10**, 1645.
23 A. A. Balandin, Thermal properties of graphene and nanostructured carbon materials, *Nat. Mater.*, 2011, **10**, 569.
24 D. L. Nika and A. A. Balandin, Two-dimensional phonon transport in graphene, *J. Phys.: Condens. Matter*, 2012, **24**, 233203.
25 D. L. Nika and A. A. Balandin, Phonons and thermal transport in graphene and graphene-based materials, *Rep. Prog. Phys.*, 2017, **80**, 036502.
26 J. Judek, A. P. Gertych, M. Świniarski, A. Łapinska, A. Dużynska and M. Zdrojek, High accuracy determination of the thermal properties of supported 2D materials, *Sci. Rep.*, 2015, **5**, 12422.
27 C. Rice, R. J. Young, R. Zan, U. Bangert, D. Wolverson, T. Georgiou, R. Jalil and K. S. Novoselov, Raman-scattering measurements and first-principles calculations of strain-induced phonon shifts in monolayer MoS_2, *Phys. Rev. B: Condens. Matter Mater. Phys.*, 2013, **87**, 081307(R).
28 H. J. Conley, B. Wang, J. I. Ziegler, R. F. Haglund Jr., S. T. Pantelides and K. I. Bolotin, Bandgap Engineering of Strained Monolayer and Bilayer MoS_2, *Nano Lett.*, 2013, **13**, 3626.
29 Y. Y. Hui, X. Liu, W. Jie, N. Y. Chan, J. Hao, Y.-T. Hsu, L.-J. Li, W. Guo and S. P. Lau, Exceptional Tunability of Band Energy in a Compressively Strained Trilayer MoS_2 Sheet, *ACS Nano*, 2013, **7**, 7126.
30 Y. Wang, C. Cong, C. Qiu and T. Yu, Raman Spectroscopy Study of Lattice Vibration and Crystallographic Orientation of Monolayer MoS_2 under Uniaxial Strain, *Small*, 2013, **17**, 2857.

 This journal is © the Owner Societies 2018

Published on 16 May 2018. Downloaded by Politechnika Warszawska on 07/06/2018 11:47:48.

31 X. Liu, I. Balla, H. Bergeron, G. P. Campbell, M. J. Bedzyk and M. C. Hersam, Rotationally Commensurate Growth of MoS_2 on Epitaxial Graphene, *ACS Nano*, 2016, **10**, 1067.
32 W. H. Chae, J. D. Cain, E. D. Hanson, A. A. Murthy and V. P. Dravid, Substrate-induced strain and charge doping in CVD-grown monolayer MoS_2, *Appl. Phys. Lett.*, 2017, **111**, 143106.
33 B. Chakraborty, A. Bera, D. V. S. Muthu, S. Bhowmick, U. V. Waghmare and A. K. Sood, Symmetry-dependent phonon renormalization in monolayer MoS_2 transistor, *Phys. Rev. B: Condens. Matter Mater. Phys.*, 2012, **85**, 161403(R).
34 C. Lee, H. Yan, L. E. Brus, T. F. Heinz, J. Hone and S. Ryu, Anomalous Lattice Vibrations of Single- and Few-Layer MoS_2, *ACS Nano*, 2010, **4**, 2695.
35 A. Michail, N. Delikoukos, J. Parthenios, C. Galiotis and K. Papagelis, Optical detection of strain and doping inhomogeneities in single layer MoS_2, *Appl. Phys. Lett.*, 2016, **108**, 173102.
36 J. Judek, A. P. Gertych, M. Krajewski, K. Czerniak, A. Łapińska, J. Sobieski and M. Zdrojek, Statistical analysis of the temperature dependence of the phonon properties in supported CVD graphene, *Carbon*, 2017, **124**, 1.
37 S. Kataria, S. Wagner, T. Cusati, A. Fortunelli, G. Iannaccone, H. Pandey, G. Fiori and M. C. Lemme, Growth-Induced Strain in Chemical Vapor Deposited Monolayer MoS_2: Experimental and Theoretical Investigation, *Adv. Mater. Interfaces*, 2017, **4**, 1700031.
38 J. E. Lee, G. Ahn, J. Shim, Y. S. Lee and S. Ryu, Optical separation of mechanical strain from charge doping in graphene, *Nat. Commun.*, 2012, **3**, 1024.
39 M. Krystek and M. Anton, A weighted total least-squares algorithm for fitting a straight line, *Meas. Sci. Technol.*, 2007, **18**, 3438.
40 B. Peng, H. Zhang, H. Shao, Y. Xu, X. Zhang and H. Zhu, Thermal conductivity of monolayer MoS_2, $MoSe_2$, and WS_2: interplay of mass effect, interatomic bonding and anharmonicity, *RSC Adv.*, 2016, **6**, 5767.
41 T. Middelmann, A. Walkov, G. Bartl and R. Schodel, Thermal expansion coefficient of single-crystal silicon from 7 K to 293 K, *Phys. Rev. B: Condens. Matter Mater. Phys.*, 2015, **92**, 174113.
42 L. Su, Y. Yu, L. Cao and Y. Zhang, Effects of substrate type and material-substrate bonding on high-temperature behavior of monolayer WS_2, *Nano Res.*, 2015, **8**, 2686.
43 P. S. Peercy and B. Morosin, Pressure and temperature dependences of the raman-active phonons in SnO_2, *Phys. Rev. B: Solid State*, 1973, **7**, 2779.
44 M. Kalbac, O. Frank and L. Kavan, Effects of heat treatment on raman spectra of two-layer 12C/13C graphene, *Chem. – Eur. J.*, 2012, **43**, 13877.
45 T. G. A. Verhagen, K. Drogowska, M. Kalbac and J. Vejperova, Temperature-induced strain and doping in monolayer and bilayer isotopically labeled graphene, *Phys. Rev. B: Condens. Matter Mater. Phys.*, 2015, **92**, 125437.